arXiv:1603.00143v1 [astro-ph.HE] 1 Mar 2016

Emergence of nonlinearity and plausible turbulence in accretion disks via hydromagnetic transient growth faster than magnetorotational instability

Sujit K. Nath* and Banibrata Mukhopadhyay**

Department of Physics, Indian Institute of Science,
Bangalore, Karnataka 560012, India
**E-mail: sujitkumar@physics.iisc.ernet.in, ** E-mail: bm@physics.iisc.ernet.in*
www.iisc.ernet.in

We investigate the evolution of hydromagnetic perturbations in a small section of accretion disks. It is known that molecular viscosity is negligible in accretion disks. Hence, it has been argued that Magnetorotational Instability (MRI) is responsible for transporting matter in the presence of weak magnetic field. However, there are some shortcomings, which question effectiveness of MRI. Now the question arises, whether other hydromagnetic effects, e.g. transient growth (TG), can play an important role to bring nonlinearity in the system, even at weak magnetic fields. Otherwise, whether MRI or TG, which is primarily responsible to reveal nonlinearity to make the flow turbulent? Our results prove explicitly that the flows with high Reynolds number (R_e), which is the case of realistic astrophysical accretion disks, exhibit nonlinearity by best TG of perturbation modes faster than that by best modes producing MRI. For a fixed wavevector, MRI dominates over transient effects, only at low R_e, lower than its value expected to be in astrophysical accretion disks, and low magnetic fields. This seriously questions (overall) persuasiveness of MRI in astrophysical accretion disks.

Keywords: Magnetohydrodynamics; Turbulence; Instability; Magnetorotational instability; Transient growth.

1. Introduction

Accretion disks are found in active galactic nuclei (AGNs), around a compact stellar object in binary systems, around newly formed stars etc.[1,2]. However, the working principle of accretion disks still remains enigmatic to us. Due to its inadequacy of molecular viscosity, turbulent viscosity has been proposed to explain the transport of matter towards the central object. This idea is particularly attractive because of its high $R_e(\gtrsim 10^{14})$[3]. However, the Keplerian disks, which are relevant to many astrophysical applications, are remarkably Rayleigh stable. Therefore, linear perturbation cannot induce the onset of turbulence and, consequently, cannot provide enough turbulent viscosity to transport matter inwards.

With the application of Magnetorotational Instability (MRI)[4,5] to Keplerian disks, Balbus & Hawley[6] showed that initial seed, weak magnetic field can lead to the velocity and magnetic field perturbations growing exponentially and reveal the onset of turbulence. However, for flows having strong magnetic fields, where the magnetic field is tightly coupled with the flow, MRI is not expected to work. Hence, it is very clear that the MRI is bounded in a small regime of parameter values when the field is weak.

It has been argued by several works that transient growth (TG) can reveal nonlinearity and transition to turbulence at sub-critical R_e[7–13]. Such sub-critical tran-

sition to turbulence was invoked to explain colder purely hydrodynamic accretion flows, e.g. in quiescent cataclysmic variables, in proto-planetary and star-forming disks, the outer region of disks in active galactic nuclei. Note that while hotter flows are expected to be ionized enough to produce weak magnetic fields therein and subsequent MRI, colder flows may remain to be practically neutral in charge and hence any instability and turbulence therein must be hydrodynamic. However, in the absence of magnetic effects, the Coriolis force does not allow any significant TG in accretion disks in three dimensions, independent of R_e [7], while in pure two dimensions TG could be large at large R_e. However, a pure two-dimensional flow is a very idealistic case. Nevertheless, in the presence of magnetic field, even in three dimensions, TG could be very large (Coriolis effects could not suppress the growth). Hence, in a real three-dimensional flow, it is very important to explore magnetic TG.

In the present paper, we explore the relative strengths of MRI and TG in magnetized accretion flows, in order to explain the generic origin of nonlinearity and plausible turbulence therein. By TG we precisely mean the short-time scale growth due to shearing perturbation waves, producing a peak followed by a dip. By MRI we mean the exponential growth by static perturbation waves. While TG may reveal nonlinearity in the system, depending on R_e, amplitude of initial perturbation and its wavevector and background rotational profile of the flow, question is, can its growth rate be fast enough to compete with that of MRI? On the other hand, is there any limitation of MRI, apart from the fact that MRI does not work at strong magnetic fields? Note that some limitations of MRI were already discussed by previous authors [12,14–17], which then question the origin of viscosity in accretion disks.

We show below that the three-dimensional TG dominates over the growth due to MRI modes at large R_e, bringing nonlinearity in the flows. By comparing modes corresponding to static (original MRI) and shearing (TG) waves, the growth estimates from static MRI waves have already been argued to be misleading [7,8]. We will show below that in a shorter time-scale, TG reveals nonlinearity into the system.

We furthurmore explicitly calculate the magnetic field strength above which MRI not working. We notice that above a threshold R_e, only TG is sufficient to make the system nonlinear at low magnetic field and there is no growth at high magnetic fields. The working regime of MRI is rather much narrower than it is generally believed. As TG was argued to be plausible source of nonlinearity in cold disks and the growth due to MRI is subdominant compared to TG at high R_e in hot disks, TG could be argued to be the source of nonlinearity and plausible turbulence and subsequent viscosity, in any accretion disk.

2. Governing Equations Describing Perturbed Magnetized Rotating Shear Flows

Within a local shearing box, in Lagrangian coordinate, the perturbed and linearized Navier-Stokes, continuity, magnetic induction equations and solenoidal condition (for magnetic field) can be written as

$$\dot{\delta\mathbf{v}} = -\frac{1}{\rho}c_s^2\nabla\delta\rho + \frac{1}{R_e}\nabla^2\delta\mathbf{v} + 2\delta\mathbf{v}\times\mathbf{\Omega} + \frac{1}{4\pi\rho}\mathbf{B}\cdot\nabla\delta\mathbf{B} + \Omega\delta\mathbf{v}\cdot\mathfrak{q}, \tag{1}$$

$$\dot{\delta\rho} = -\rho\nabla\cdot\delta\mathbf{v}, \tag{2}$$

$$\dot{\delta\mathbf{B}} = \nabla\times(\mathbf{v}\times\delta\mathbf{B} + \delta\mathbf{v}\times\mathbf{B}) + (\mathbf{v}\cdot\nabla)\delta\mathbf{B}, \quad \nabla\cdot\delta\mathbf{B} = 0, \tag{3}$$

where $\mathbf{v}$, $\mathbf{B}$, Ω, ρ, c_s and R_e are the background velocity, magnetic field vectors, angular velocity, density, sound speed and Reynolds number respectively and the quantities with δ such as $\delta\mathbf{v}$, $\delta\mathbf{B}$ etc. are the respective perturbed quantities. $\mathfrak{q}$ is the tensor related to the background shearing velocity depending on the rotation parameter q[8]. Here we take the background shearing velocity as $\mathbf{v} = (0, -q\Omega x, 0)$, where x is the x-component of the Cartesian position vector of a fluid element inside the shearing box.

We now work with the incompressible approximation, i.e. $\delta\rho \to 0$ and $c_s^2 \to \infty$, assuming $c_s^2\delta\rho$ to be finite and decompose the general linear perturbations into a plane wave form as

$$\delta\mathbf{v}, \delta\mathbf{B} \propto exp(i\mathbf{k}^L\cdot\mathbf{r}^L), \tag{4}$$

when

$$\mathbf{k} = (k_x, k_y, k_z) = (\mathbf{1} + \Omega t\mathfrak{q})\cdot\mathbf{k}^L = (k_x^L + q\Omega t k_y^L, k_y^L, k_z^L), \tag{5}$$

where $\mathbf{k}$ and $\mathbf{k}^L$ are the wavevectors in the Eulerian and Lagrangian coordinates respectively and t is the time. Now solving equations (1), (2) and (3) and using (4) we calculate energy of the perturbation and linearity given by

$$\mathcal{E} \propto \left(\delta\mathbf{v}^2 + \frac{\delta\mathbf{B}^2}{4\pi\rho}\right), \quad \text{Linearity} = \left(\frac{|\delta\mathbf{v}|}{|\mathbf{v}|} + \frac{|\delta\mathbf{B}|}{|\mathbf{B}|}\right) \tag{6}$$

respectively, when $|\delta\mathbf{v}|/|\mathbf{v}|$, $|\delta\mathbf{B}|/|\mathbf{B}|$ at time $t = 0$ are respective initial perturbation amplitude (IPA). For other details, see Ref. 19.

3. Total Energy Growth and Nonlinearity of Perturbations for Different Parameter Values

The best possible mode for MRI giving rise to the nonlinearity in the system corresponds to the condition $k_z v_{Az}/\Omega = 1$, when $v_{Az}^2 = B_z^2/4\pi\rho$, is the Alfvén velocity[6]. The growth rate for this fastest exponentially growing mode is $3\Omega/4 = 3/4q$ (since in dimensionless unit $\Omega = 1/q$)[6,7,18]. Note that an approximate emergence of nonlinearity is defined through the measurement of the quantity "Linearity"as defined

in eq. (6). When Linearity = 1, the system will start becoming nonlinear which will plausibly lead to turbulence. For a Keplerian disk ($q = 3/2$), the best MRI mode brings in the nonlinearity at the timescales ~ 14 and 23 rotation times respectively for IPAs $= 10^{-3}$ and 10^{-5}. However Fig. 1a shows that there are modes which reveal nonlinearity via TG following eqn. (6) at around 3 and 13 rotational times for IPAs 10^{-3} and 10^{-5} respectively or even less (Fig. 1b), which shows faster growth rates than MRI. In Fig. 1c we show the total energy growth of perturbation for different strengths of magnetic fields. Thick and long dashed lines correspond to relatively stronger magnetic fields for which there is eventually no energy growth and the system remains linear and stable. Dotted and dot-dashed lines correspond to weaker magnetic fields for which the total energy starts growing and makes the system nonlinear and plausibly unstable. Also it is seen that *for a given shearing mode*, in case of weak magnetic fields, nonlinearity comes through MRI for low R_e, and via TG for high R_e, which are the cases for astrophysical accretion disks.

4. Calculation of the Threshold Value of Magnetic Field Strength supporting instability

Let us estimate the maximum $|\mathbf{B}|$ in Gauss supporting nonlinearity, as shown by the solid curve in Fig. 1d. We set the shearing box at $100R_g$ away from a $10M_\odot$ black hole. Then we obtain the values of density (ρ_{100R_g}) at that location to be $\sim 10^{-4}$ gm/cc^2. The background Keplerian velocity at that position, for the size of the shearing box, $0.1R_g$, which is consistent with that obtained for the TG active zone[19], can be obtained as $q\Omega L = q\sqrt{GM/R^3}L \sim 10^6$ cm/sec. We now consider $R_e = 10^{12}$ and, hence, from the solid line of Fig. 1d the corresponding maximum (dimensionless) magnetic field supporting nonlinearity is given by $B^2/\rho = 10^{-5}$. Therefore, corresponding actual value of magnetic field is $\sqrt{10^{-5}\rho_{100R_g}(q\Omega L)^2} \sim 30$ Gauss. This means, the flow with $R_e = 10^{12}$ and $|\mathbf{B}| > 30$ Gauss, the energy growth of perturbation will decay over time, but for $|\mathbf{B}| \leqslant 30$ Gauss, TG will be sufficient enough to bring nonlinearity in the system, however, still not requiring any growth due to MRI. From Fig. 1d, it is clear that MRI is only important whenever $R_e < 10^9$, whereas for $R_e \geqslant 10^9$, which is the favorable zone of R_e for accretion disks, magnetic TG is important than MRI.

5. Conclusions

Here we have shown that, in accretion disks, there are TG modes, which bring nonlinearity faster than the best possible MRI mode. We have computed the magnetic field strengths for different R_es above which the system will be stable under linear perturbation. We have also calculated, for a given shearing mode, an upper bound of R_e above which either the system is stable under linear perturbation (for high magnetic field strength) or reaches nonlinear regime (for low magnetic field) through magnetic TG (Fig. 1d). Since astrophysical accretion flows have high R_e

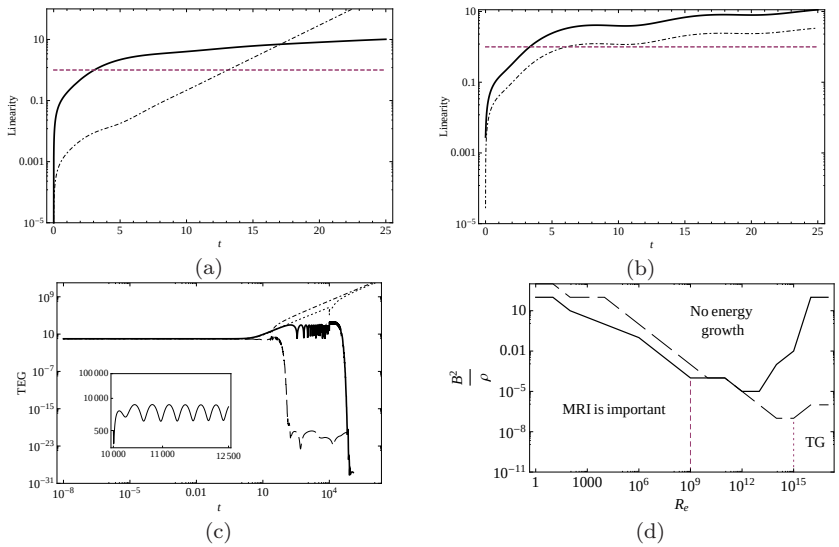

Fig. 1. (a) Nonlinearity via best possible TG and MRI. Thick black line corresponds to the TG for IPA= 10^{-3}, $R_e = 10^{14}$, $k_x^L = -Re^{1/3}$, $k_y = 1$, $k_z = 90K_x^L$; dotdashed black line corresponds to the TG for IPA= 10^{-5}, $R_e = 10^{25}$, $k_x^L = -Re^{1/3}$, $k_y = 1$, $k_z = 90k_x^L$; red longdashed and dotted lines correspond to the best possible MRI for IPA = 10^{-3} and 10^{-5} respectively. Dashed horizontal line indicates linearity unity. (b) Same as (a), but the black thick and dotdashed lines correspond to TG for $k_x^L = 1$, $k_y = 1$, $k_z = 100$, $R_e = 10^{12}$ and $k_x^L = 1$, $k_y = 1$, $k_z = 3000$, $R_e = 10^{12}$ respectively. (c) Total energy growth for different sets of R_e and $\mathbf{B} = (0, 0, B_3)$ for $k_x^L = -Re^{1/3}$, $k_y = k_z = 1$: Thick, longdashed, dotted and dotdashed lines correspond to respectively $R_e = 10^{12}$ and $B^2/\rho = 10^{-3}$; $R_e = 10^4$ and $B^2/\rho = 10$; $R_e = 10^{12}$ and $B^2/\rho = 10^{-20}$; and $R_e = 10^4$ and $B^2/\rho = 10^{-20}$. Inset confirms that the oscillatory zone of thick line is continuous and smooth. (d) Parameter space describing stable and unstable zones, based on the MRI and TG inactive and active regions, for $k_x^L = -Re^{1/3}$, $k_y = k_z = 1$, $\mathbf{B} = (0, 0, B_3)$. Solid and longdashed lines are for IPA = 10^{-3} and 10^{-5} respectively. The dashed and dotted vertical lines at $R_e = 10^9$ and 10^{15} correspond to boundary R_e for the cases IPA = 10^{-3} and 10^{-5} respectively.

$(\gtrsim 10^{14})$[3], it becomes nonlinear plausibly by magnetic TG. Hence, MRI is not the sole mechanism to make accretion disk unstable, there is a large area where TG rules, and explanation of accretion solely via MRI is misleading.

References

1. J.E. Pringle, *ARA&A* **19,** 137 (1981).
2. N.I. Shakura and R.A. Sunyaev, *Astron. Astrophys.* **86,** 337 (1973).
3. B. Mukhopadhyay, *Phys. Lett. B* **721,** 151 (2013).
4. E. Velikhov, *J. Exp. Theor. Phys.* **36,** 1398 (1959).
5. S. Chandrasekhar, *Proc. Nat. Acad. Sci.* **46,** 53 (1960).
6. S.A. Balbus and J.F. Hawley, *Astrophys. J.* **376,** 214 (1991).
7. B. Mukhopadhyay, N. Afshordi and R. Narayan, *Astrophys. J.* **629,** 383 (2005).

8. N. Afshordi, B. Mukhopadhyay and R. Narayan, *Astrophys. J.* **629,** 373 (2005).
9. G.D. Chagelishvili, J.-P. Zahn, A.G. Tevzadze and J.G. Lominadze, *Astron. Astrophys.* **402,** 401 (2003).
10. P.A. Yecko, *Astron. Astrophys.* **425,** 385 (2004).
11. O.M. Umurhan and O. Regev, *Astron. Astrophys.* **427,** 855 (2004).
12. M. Avila, *Phys. Rev. Lett.* **108,** 124501 (2012).
13. H.H. Klahr and P. Bodenheimer, *Astrophys. J.* **582,** 869 (2003).
14. S.M. Mahajan and V. Krishan, *Astrophys. J.* **682,** 602-607 (2008).
15. O.M. Umurhan, K. Menou and O. Regev, *Phys. Rev. Lett.* **98,** 034501 (2007).
16. E. Liverts, Y. Shtemler, M. Mond, O.M. Umurhan and D.V. Bisikalo, *Phys. Rev. Lett.* **109,** 224501 (2012).
17. M.E. Pessah and C. Chan, *Astrophys. J.* **751,** 48 (2012).
18. S.A. Balbus and J.F. Hawley, *Rev. Mod. Phys.* **70,** 1 (1998).
19. S.K. Nath and B. Mukhopadhyay, *Phys. Rev. E* **92,** 023005 (2015).